Science of the Total Environment 784 (2021) 146995

Contents lists available at ScienceDirect

Science of the Total Environment

journal homepage: www.elsevier.com/locate/scitotenv

Thallium geochemical fractionation and migration in Tl-As rich soils: The key controls

Xudong Wei [a,e], Jin Wang [a], Jingye She [a], Jing Sun [b], Juan Liu [a,*], Yuxuan Wang [a], Xiao Yang [c], Qi"en Ouyang [a], Yuyang Lin [a], Tangfu Xiao [a], Daniel C.W. Tsang [d]

[a] Key Laboratory of Water Quality and Conservation in the Pearl River Delta, Guangdong Provincial Key Laboratory of Radionuclides Pollution Control and Resource, School of Environmental Science and Engineering, Guangzhou University, Guangzhou 510006, China
[b] State Key Laboratory of Environmental Geochemistry, Institute of Geochemistry, Chinese Academy of Sciences, Guiyang 550081, China
[c] Key Laboratory of Land Surface Pattern and Simulation, Institute of Geographic Sciences and Natural Resources Research, Chinese Academy of Sciences, Beijing 100101, China
[d] Department of Civil and Environmental Engineering, The Hong Kong Polytechnic University, Hung Hom, Kowloon, Hong Kong, China
[e] Department of Agronomy, Food, Natural resources, Animals and Environment (DAFNAE), University of Padua, Agripolis Campus, Viale dell'Università, 16, 35020 Legnaro, PD, Italy

HIGHLIGHTS

- Half of geochemically mobile fraction of thallium (Tl) was observed in the topsoils.
- Dominant portion (29%) of mobile Tl was enriched in the reducible fraction.
- Participation of Fe oxides plays a critical role in generating highly elevated mobile Tl.
- LA-ICP-MS and TEM revealed Tl translocation pathway from tailings to soil profile.

GRAPHICAL ABSTRACT

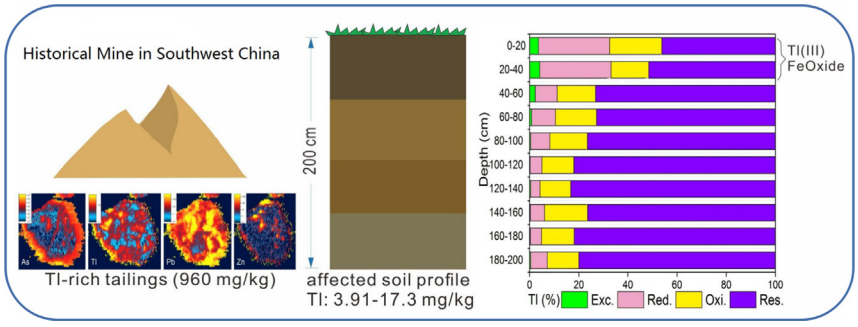

ARTICLE INFO

Article history:
Received 26 January 2021
Received in revised form 13 March 2021
Accepted 3 April 2021
Available online 9 April 2021

Editor: Xinbin Feng

Keywords:
Geochemical fractionation
Tl-As in soil
LA-ICP-MS
Metal/metalloid speciation
Mine tailings contamination

ABSTRACT

Thallium (Tl) pollution caused by mining and processing of Tl-enriched ores has become an increasing concern. This study explored the geochemical fractionation and vertical transfer of Tl in a soil profile (200 cm) from a representative Tl-As mineralized area, Southwest China. The results showed that the soils were heavily enriched by Tl and As, with concentration ranging from 3.91–17.3 and 1830–8840 mg/kg (6.79 and 2973 mg/kg in average), respectively. Approximately 50% of Tl occurred in geochemically mobile fractions in the topsoil, wherein the reducible fraction was the most enriched fraction. Further characterization using LA-ICP-MS and TEM revealed that enriched Tl and As in soils were mainly inherited from the weathering of mine tailing piles upstream. XPS characterization indicated that Fe oxides herein may play a critical role in the oxidation of Tl(I) to Tl(III) which provoked further adsorption of Tl onto Fe oxides, thereby facilitating Tl enrichment in the reducible fraction. The findings highlight that the pivotal role of Fe oxides from mineralized area in the co-mobility and migration of Tl and As in the depth profile.

1. Introduction

Thallium (Tl) is a highly toxic element that has gained worldwide concerns over the last few decades. Compared with other traditional toxic metal(loid)s such as As and Cr, Tl is remarkably more poisonous and causes damage both to gastrointestinal, muscular and nervous

* Corresponding author.
E-mail address: liujuan858585@163.com (J. Liu).

https://doi.org/10.1016/j.scitotenv.2021.146995
0048-9697/

systems (Vaněk et al., 2013; Qi et al., 2019; Liu et al., 2019a,b, 2021; Yin et al., 2021). Thallium concentration in the natural environment is generally low, with 0.52 mg/kg in the Earth's crust and 0.012–0.016 μg/L in seawater (Xiao et al., 2012; Liu et al., 2018; George et al., 2019). However, as a chalcophile element, Tl is generally enriched in sulfidic minerals, such as FeS_2, PbS, ZnS and As_2S_3 (Xiao et al., 2012; Belzile and Chen, 2017; Liu et al., 2020c,d; Vaněk et al., 2018). In recent years, an increasing utilization of Tl-rich minerals has resulted in Tl-related pollution events in many typical mining/smelting areas worldwide (Lukaszewski et al., 2018; Vaněk et al., 2019; Wang et al., 2020b; Wei et al., 2020). Previous studies found that Tl was dispersed into acid mine drainage, river, sediment, tap water, soil, air, plants and animals around mining areas through multiple natural or anthropogenic pathways, posing threats to the local environment (Liu et al., 2020b; Vaněk et al., 2016; Wang et al., 2020c, 2021a; Zhou et al., 2021).

Arsenic (As) is a widely distributed element in the environment and also enriched in sulfidic minerals (Besold et al., 2018; Beiyuan et al., 2017b; Wang et al., 2020a). As poisoning can cause blackfoot disease, polyneuritis and mental disorder (Rahman et al., 2018; Wu et al., 2020). Compared with Tl, As has been well-known for its poisonous effects for more than a century and captured a lot of research attentions (Alvarenga et al., 2019; Kaya et al., 2020; Sun et al., 2016; Verma et al., 2020). Pertinent studies on As contamination have been carried out and improve our understanding of As contamination in soils and plants and its effects both to the environment and to the human beings (Meharg and Rahman, 2003; Carrizales et al., 2006; Rocke, 2013; Alloway, 2015; Beiyuan et al., 2017a).

Recent studies have found that utilization of As-Tl enriched minerals generates Tl-As pollution in the Republic of Macedonia, Swiss, Spain and China (López-Arce et al., 2019; Wei et al., 2020). In China, the southwestern region is of great importance for industrial production and provides large amounts of metal-enriched ores per year (Xiao et al., 2012; Liu et al., 2019a). Our previous study focused on a historical mine for As_2O_3 production during the year of 1960–2000 in Southwest China and found that the soils and plants, brake fern (*Pteris vittata* L.), around the mining area were heavily contaminated by both Tl and As (Wei et al., 2020). Tl in the topsoil may influence survival and metabolisms of microorganisms, soil animals and plants, whereas Tl in deeper soil may cause Tl contamination in the groundwater (Xiao et al., 2003; Ghezzi et al., 2019; Wei et al., 2020; Wick et al., 2020). Previous studies have shown that geochemical migration of thallium in soils was regulated by speciation and fractionation (Voegelin et al., 2015; Li et al., 2020; Lin et al., 2020). However, limited information is available concerning the speciation and extractability of Tl and co-contamination mechanism of Tl and As in the environment, especially for the Tl-As co-contaminated soil profile.

A series of soils from different layers of a Tl-As co-contaminated profile (depth of 200 cm) were collected from a mine tailings-affected area in Southwest China to implement this study. The main objectives of this study were (i) to uncover the contents and dispersing trend of Tl and associated elements throughout vertical profile, (ii) to reveal Tl geochemical fractionation in the soil profile (iii) to study the geochemical potential mobility of Tl based on its mineralogical characteristics, micro/nano distribution, geochemical fractionation and speciation. This study highlights the fate of Tl-As co-contamination in topsoil near a typical mine tailings abandoned area, which is critical for understanding the geochemical fate of Tl and advising future remediation of Tl pollution.

2. Materials and methods

2.1. Sampling site

The sampling site (24°57′ N and 101°15′ E) was located, around a historical arsenic mine in Nanhua County, the southwestern of Yunnan province, which was found enriched in both As and Tl (Wei et al., 2020). Before discontinued in 2000, the mining activities had produced 2000 tons of As_2O_3 and a large amount of mine tailings and wastes were also generated. Mine tailings without treatment were stacked around the entrance of the mining valley. The hill-shaped tailings had mostly bare surface and limited vegetation with only several kinds of herbaceous plants. A soil profile was collected from a site that was 20 m from the mine tailings storage site (which was also be collected). The soil surface was covered by the brake ferns (*Pteris vittata* L.) and the sampling profile was 200 cm deep. A total of 10 bulk soil samples with ~10 kg per sample were collected using a stainless steel hand shovel at intervals of 20 cm. The pretreatment method for drying and grinding soil samples was based on a previous procedure by Liu et al. (2020a). In brief, the soil samples were stored in plastic bags and later dried in an oven at 70 °C to constant weight, ground to powder using an agate mortar and sieved to <80 μm in diameter.

2.2. Bulk, geochemical fractionation and speciation analysis

To determine the elemental composition of the samples, each soil or ore sample (100 mg) was added into a mixture of 68% HNO_3 (10 mL) and 48% HF (5 mL) at 150 °C in a Teflon vessel for digestion (Liu et al., 2020a; Wang et al., 2021b). The suspension was evaporated to dryness, with redissolution in HNO_3 (8 M) and dilution in Milli-Q water (HNO_3/water = 1/4). The digests were analyzed by Inductively Coupled Plasma Mass Spectrometer (ICP-MS, PE-Sciex Elan 6100 DRC-II, Perkin Elmer, US) (Voegelin et al., 2015; Wei et al., 2020; Yin et al., 2019, 2020). Certified reference materials (GBW07446 (Chinese soils)), triplicate samples, and reagent blanks/controls were used to assure the accuracy of the experimental data. The relative standard deviation (RSD) of each element was less than 5.0%.

Tl geochemical fractionation was determined according to the IRMM sequential extraction method with four different fractions, including acid exchangeable, reducible, oxidizable and residual fractions (Lin et al., 2020). For exchangeable fraction, 500 mg of soil was added into 20 mL 0.11 mol/L CH_3COOH for extraction (16 h) at room temperature in a constantly agitated polyethylene centrifuge tube. For reducible fraction, residue from step 1 was extracted with 20 mL 0.5 mol/L $NH_2OH{\cdot}HCl$ for 16 h at room temperature in a constantly agitated polyethylene centrifuge tube. For oxidizable fraction, the residue from step 2 was extracted twice with 5 mL 8.8 mol/L H_2O_2 (pH 2.2) at 85 °C for 2 h followed by a 16 h extraction with 1 mol/L CH_3COONH_4 (pH 2.0) at 25 °C. The residue from step 3 representing the residual fraction was then digested in a mixture of HNO_3 and HF.

2.3. TEM, LA-ICP-MS and XPS analysis

To investigate the elemental distribution at nano/micro-scale, the soil/mine tailing samples were analyzed by Transmission Electron Microscope (TEM, JEOL JEM-2100F), equipped with an Energy Dispersive Spectrometer (EDS, Oxford Instruments) and High Resolution Transmission Electron Microscope (HRTEM, 200 kV) (Wei et al., 2020). The HRTEM images (10 nm) were analyzed by Fast Fourier Transformation (FFT) to produce the Electron Microscope (EM) maps (Wei et al., 2020). Digital Micrograph was used to obtain d-spacing and axis degrees of (FFT) image and (EM) maps (Downs and Hall-Wallace, 2003; Yin et al., 2019). Then the data was handled according to the American Mineralogist Crystal Structure Database to determine its mineralogical composition (Downs and Hall-Wallace, 2003).

Laser Ablation Inductively Coupled Plasma Mass Spectrometry (LA-ICP-MS) was used for concentration measurements and analysis of micro/nano distribution of elements in the mine tailings. Data were collected by an NWR193UC 193 nm Excimer Laser attached to a Thermo Scientific iCAP RQ ICP-MS following the methods of George et al. (2018). The laser beam spot and repetition rate were 10 μm and 20 Hz, respectively, for mapping and the scanning rate was 20 μm/s. Standard material NIST 610 was used for calibration and Software iolite was

Table 1
Contents of elements (mg/kg) in soils.

	Tl	As	Pb	Zn	Sb	Cd	Cr	Fe	Ni	Mn
1–20 cm	11.90 ± 0.36	8840 ± 177	1620 ± 49	1330 ± 53	1.20 ± 0.05	3.39 ± 0.14	95 ± 3.1	52,100 ± 1500	63.3 ± 2.5	643 ± 13
20–40 cm	17.30 ± 0.52	3080 ± 62	620 ± 19	671 ± 27	1.19 ± 0.04	1.74 ± 0.07	96 ± 3.0	50,200 ± 1440	61.7 ± 2.5	805 ± 26
40–60 cm	4.29 ± 0.13	2070 ± 41	209 ± 6	340 ± 14	1.10 ± 0.03	1.16 ± 0.05	97 ± 3.1	50,500 ± 1503	63.6 ± 2.4	823 ± 14
60–80 cm	4.23 ± 0.13	2100 ± 42	188 ± 6	294 ± 12	1.15 ± 0.03	1.68 ± 0.07	98 ± 2.9	50,400 ± 1400	66.6 ± 2.3	745 ± 13
80–100 cm	4.50 ± 0.14	2140 ± 43	160 ± 5	282 ± 11	1.27 ± 0.04	1.17 ± 0.04	103 ± 2.9	53,300 ± 1443	65.4 ± 2.4	708 ± 25
100–120 cm	5.09 ± 0.15	2600 ± 52	111 ± 3	213 ± 9	1.12 ± 0.03	1.54 ± 0.04	100 ± 2.8	50,900 ± 1490	63.9 ± 2.7	780 ± 15
120–140 cm	5.71 ± 0.17	2350 ± 47	144 ± 4	276 ± 11	1.15 ± 0.05	1.48 ± 0.04	98 ± 3.0	52,000 ± 1495	63.5 ± 2.6	873 ± 24
140–160 cm	3.91 ± 0.12	2560 ± 51	199 ± 6	268 ± 11	1.12 ± 0.06	1.50 ± 0.05	97 ± 2.9	53,900 ± 1407	65.8 ± 1.3	827 ± 23
160–180 cm	5.14 ± 0.15	2160 ± 43	221 ± 7	337 ± 13	1.65 ± 0.07	5.99 ± 0.24	90 ± 2.9	47,300 ± 1200	86.2 ± 2.6	855 ± 16
180–200 cm	5.83 ± 0.17	1830 ± 37	166 ± 5	362 ± 14	1.96 ± 0.05	16.30 ± 0.65	60 ± 1.8	37,900 ± 1135	55.8 ± 1.1	723 ± 17
Minimum	3.91 ± 0.12	1830 ± 37	111 ± 3	213 ± 9	1.10 ± 0.03	1.48 ± 0.04	60 ± 1.8	37,900 ± 1135	55.8 ± 1.1	643 ± 13
Maximum	17.3 ± 0.52	8840 ± 177	1620 ± 49	1330 ± 53	1.96 ± 0.05	16.30 ± 0.65	103 ± 2.9	53,900 ± 1407	86.2 ± 2.6	873 ± 24
Mean	6.79 ± 2.04	2973 ± 595	364 ± 109	437 ± 175	1.29 ± 0.52	3.60 ± 1.44	93.4 ± 28	49,850 ± 14,955	65.6 ± 26	778 ± 156
Mine tailing[a]	960 ± 19	555,300 ± 1400	205 ± 2	525 ± 11	0.71 ± 0.03	6.77 ± 0.1	16 ± 1	7800 ± 234	20.0 ± 0.4	280 ± 8
Background soil in China[b]	0.62	11.2	26	74.2	1.21	0.10	61	/	26.9	583
Maximum permissible level in soil[c]	1	30	90	200	20	0.30	64	/	70.0	1200

[a] Values are taken from Wei et al. (2020);
[b] Values are taken from CEMS (1990) and Wang et al. (1995).
[c] Values are taken from SEP and GAQIQ State Environmental Protection Administration of the P.R. China & General Administration of Quality Supervision, Inspection and Quarantine of the P. R. China, 2015.

used for the selection of samples and blank signals, the sensitivity drift correction and the element content calculation. The LA-ICP-MS mapping was used to monitor the variation and zonation of trace elements such as As, Tl, Pb, etc. To gain the information of valence states, soil was tested by an X-ray Photoelectron Spectroscopy (XPS, Thermo Fisher ESCALAB 250Xi, X-ray source: Mono AlKa, at 1486.6 eV) and data was analyzed by XPS Peak.

2.4. Statistical analysis

Spearman correlation analysis was performed to reveal the relationships of Tl with the other elements including As, Pb, Zn, Sb, Fe and Mn in the soil profile. The correlations of Tl geochemical fractionations and the bulk contents were also analyzed. SPSS Statistics version 19.0 was used for statistical analyses.

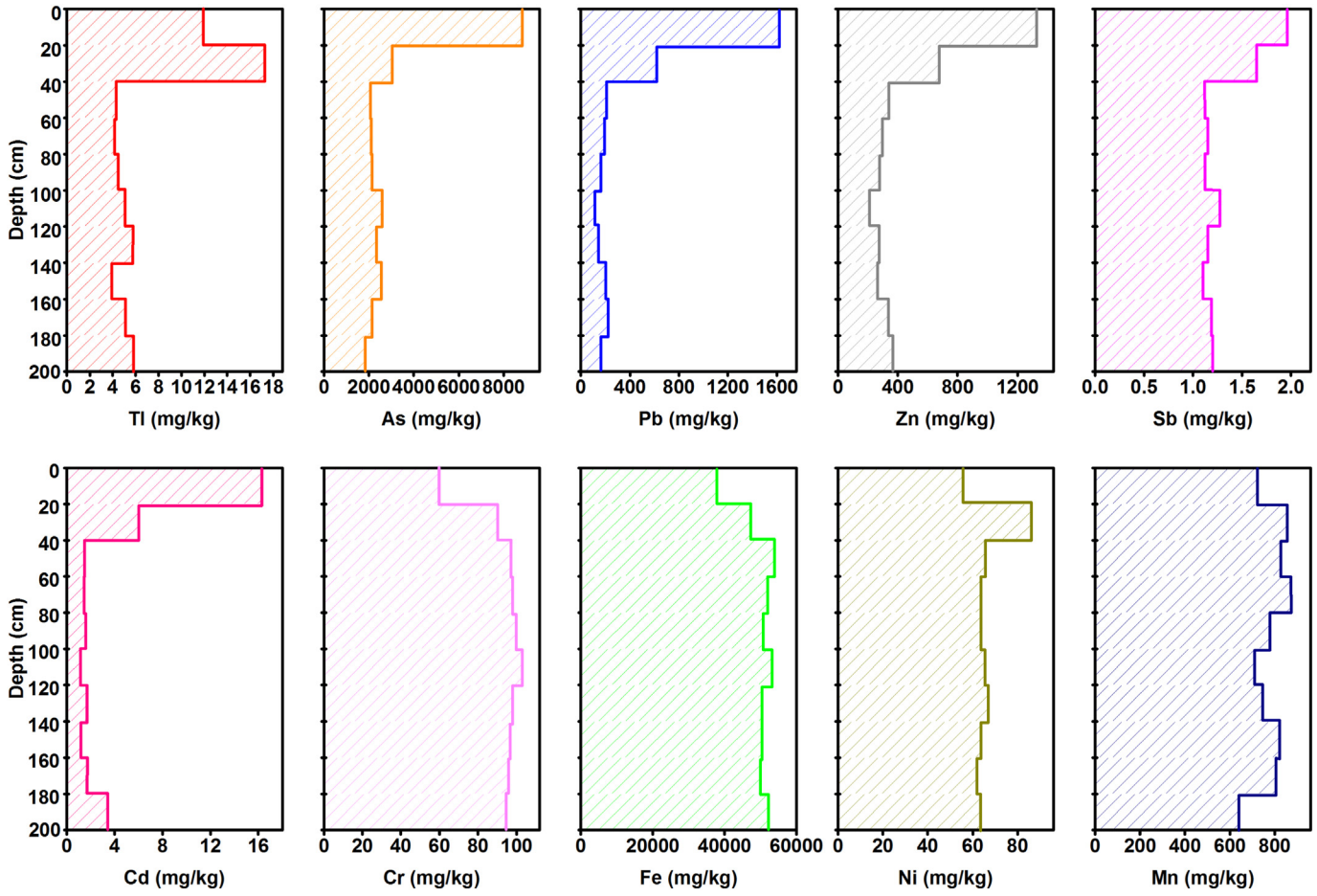

Fig. 1. Elements contents of the soil profile.

3. Results and discussion

3.1. Elements distribution

As displayed in Table 1, the contents of Tl in the soil profile with a total length of 200 cm (20 cm per layer) were within 3.91 to 17.3 mg/kg, far exceeding the content in the background soil of China (0.62 mg/kg) (CEMS, 1990). It also exceeded the maximum permissible level (MPL) for soil in China (1 mg/kg) (SEP and GAQIQ State Environmental Protection Administration of the P.R. China & General Administration of Quality Supervision, Inspection and Quarantine of the P. R. China, 2015). The contents of Tl in this Tl-As co-contaminated soil profile were much higher than those in soils from South China and East China (less than 15 mg/kg), steel smelting area in Guangdong Province, China (0.9–1.8 mg/kg), and a Cu industrial production region in Fujian Province, China (0.6–3.3 mg/kg) (Yang et al., 2005; Zhou et al., 2007; Liu et al., 2017; Guo et al., 2018). Compared with Tl levels of those in severely contaminated soils from Linares smelting area, Spain (0.5–39.5 mg/kg) (Cortada et al., 2018) and Lanmuchang mining district, China (181 mg/kg) (Lin et al., 2020; Wang et al., 2018a), Tl contamination in soils from the studied area was moderate. However, the mining affected soils in this study were characterized by extremely high levels of As (8840 mg/kg, 0–20 cm), along with Pb (1620 mg/kg, 0–20 cm) in the surface layer.

Arsenic in the profile ranged from 1830 to 8840 mg/kg (2973 mg/kg on average), 100 times as its MPL (30 mg/kg) in soil (SEP and GAQIQ State Environmental Protection Administration of the P.R. China & General Administration of Quality Supervision, Inspection and Quarantine of the P. R. China, 2015). Arsenic in the topsoil was also higher than those reported in the soil from the LMC Tl-Hg-As mine, China (304–1480 mg/kg), (Tl,As)-rich ore meadow, Swiss (320–2270 mg/kg), and Tl, Sb, As-rich pyrite, Italy (Voegelin et al., 2015; George et al., 2019; Lin et al., 2020). In addition, the mean values of Pb, Zn, Cd and Cr (364, 437, 3.60 and 93.4 mg/kg, respectively) were also over their background values in China and their corresponding MPLs (90, 200, 0.30 and 64 mg/kg, respectively). The results indicated that the whole soil profile, even at the soil depth of 200 cm, was severely polluted by Tl, As and Pb (SEP and GAQIQ State Environmental Protection Administration of the P.R. China & General Administration of Quality Supervision, Inspection and Quarantine of the P. R. China, 2015).

As shown in Fig. 1, the topsoil (0–40 cm) contained the highest level of Tl, with 11.9 mg/kg at 0–20 cm and 17.3 mg/kg at 20–40 cm, while soil layers at the depth of 40–200 cm of the profile displayed a decreasing level of Tl (less than 6 mg/kg). As for arsenic, the highest level appeared at the depth of 0–20 cm (8840 mg/kg) and 20–40 cm (3080 mg/kg), while the contents at depth of 40–200 cm were consistently at about 2000 mg/kg. Similar to arsenic, the contents of Pb, Zn, Sb and Cd at the depth of 0–20 cm and 20–40 cm were extremely high (Pb: 1620 and 620 mg/kg; Zn: 1330 and 671 mg/kg; Sb: 1.96 and 1.65 mg/kg; Cd: 16.3 and 5.99 mg/kg) and then decreased in the deeper soil layers (40–200 cm) with steady levels. As displayed in Fig. S1, Tl showed positive relationships with Zn, Sb and Cd, which suggested that Tl, Zn, Sb and Cd in soil may be accumulated and transported similarly to the bottom layer. In contrast, the contents of Cr, Ni, Fe and Mn in the soil profile remained relatively constant across the depth. The results indicated a tremendous metal(loid)s contamination in the topsoil of this mining area, due to the weathering and leaching of mine tailings (Tl = 960 mg/kg). Tl and As in the topsoil might induce toxic metal(loid)s accumulation in the plants and pose threat to animals that consume these plants or their fruits (Briki et al., 2017; Wei et al., 2020). Moreover, those toxic metal(loid)s in deeper soil (40–200 cm) might be slowly released into pore water and cause dispersion of metal(loid)s in the groundwater (Xiao et al., 2003; Ghezzi et al., 2019; Sun et al., 2018; Wick et al., 2020).

3.2. Geochemical fractionation of Tl in soil

In order to determine the geochemical fractionation of Tl in soil, a modified IRMM sequential extraction method was used and the recovery rates ranged from 88.8% to 101.3%. Fig. 2(a) showed that Tl in the

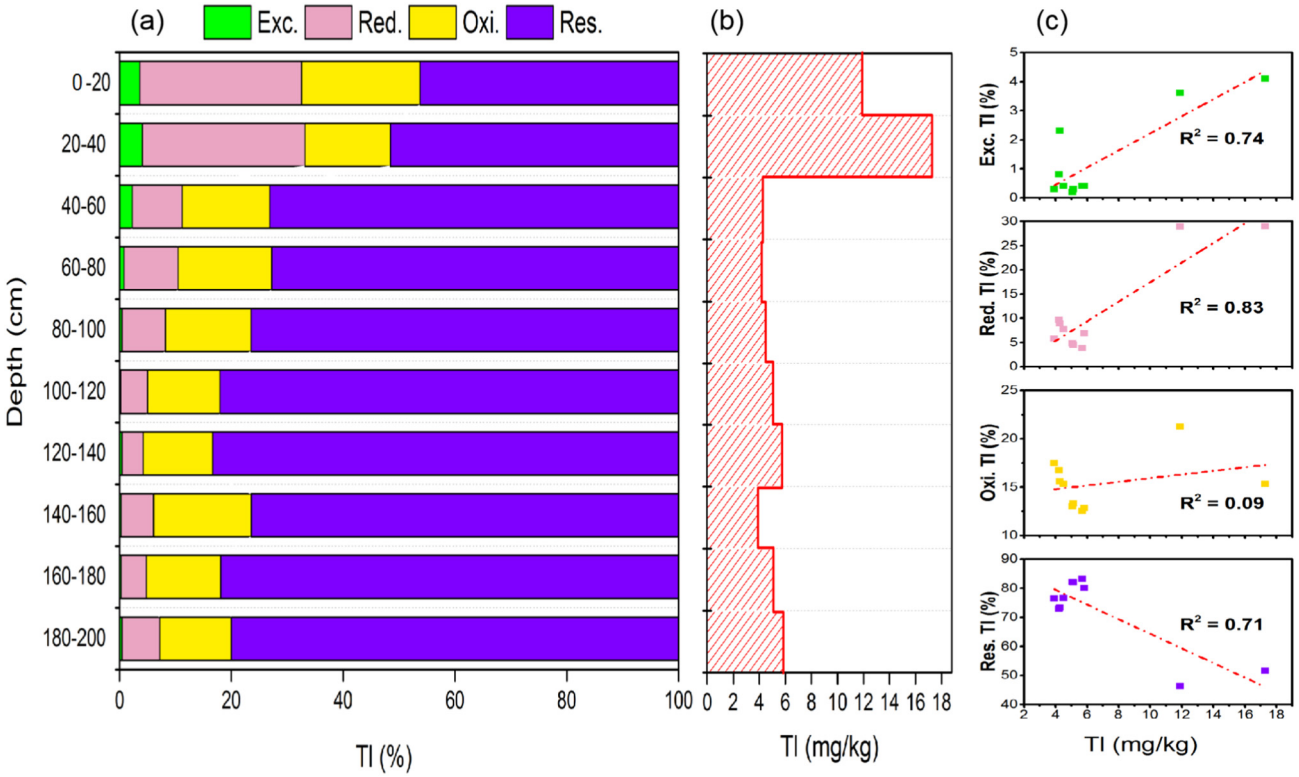

Fig. 2. Geochemical fractionation of Tl in the soils: (a) percentages of Exc./Red./Oxi./Res. fractions; (b) total contents of Tl; (c) correlation between Tl contents and different fractions.

soil profile (on average) dominantly existed as residual fraction (72.4%), followed by the oxidizable, reducible and exchangeable fractions (15.3%, 11.0% and 1.30%). The contents of Tl in the residual fraction ranged from 2.98 to 8.91 mg/kg, occupying 46.2%–83.3% of the total Tl. This result was consistent with other studies, which reported that residual fraction was the predominant fraction of Tl in the environment (Vaněk et al., 2013; Lee et al., 2015; Aguilar-Carrillo et al., 2018; Li et al., 2020).

As exhibited in Fig. 2, Tl in the reducible fraction ranged from 3.83% to 29.0%, decreasing from the top to the bottom. Tl in the exchangeable fraction was the least and shared a similar distribution pattern as Tl in the reducible fraction. It was shown that Tl in these two fractions were featured by a significant linear correlation with Tl contents ($R^2 = 0.74$ and $R^2 = 0.83$, $p < 0.01$) (Fig. 2 (c)). The results indicated that Tl in these two fractions possessed a strong relationship with original Tl contents and may share an identical geochemical migration pathway (Huang et al., 2018). Different from Tl in the reducible and exchangeable fractions, Tl in the oxidizable fraction rarely changed across the vertical soil depth, about 15.3% on average.

It is worth noting that Tl in the exchangeable, oxidizable and reducible fractions were regarded as geochemically mobile (Li et al., 2020; Lin et al., 2020). Tl in geochemically mobile fractions were within 16.7%–53.8%, and were 53.8% in 0–20 cm and 48.5% in 20–40 cm, indicating a noticeable amount of geochemically mobile Tl in the topsoil. As shown in Fig. 2, the topsoil with high Tl content was mostly enriched in the reducible fraction (0–40 cm, 29.0%), followed by exchangeable (0–40 cm, 3.88%) fraction. Fig. S2 displayed that Tl in geochemically mobile fractionation held significant linear correlation with Tl in the reducible fraction ($R^2 = 0.98$), suggesting that Tl in the reducible fraction played an important role in geochemical migration of Tl in the studied area (Lee et al., 2015).

Tl in the reducible fraction was normally integrated with Fe and Mn oxides (Aguilar-Carrillo et al., 2018; Huang et al., 2018). Oxidation of Tl(I) to Tl(III) promotes adsorption of Tl onto Fe or Mn oxides (Voegelin et al., 2015; Antić-Mladenović et al., 2017). As displayed in Table 1, the soil profile was enriched in Fe. To find out why Tl was enriched in reducible fraction and how it works, it would be critical to check if abundant Fe (or Mn) oxides (e.g., hematite, confirmed by TEM analysis) and oxidization of Tl(I) to Tl(III) (XPS analysis) were in the soil.

3.3. LA-ICP-MS and TEM analysis of mine tailings

As shown in TEM mapping (top two rows in Fig. 3), Tl, As, Pb and O were evenly scattered on the particle (1 μm) of the mine tailings and their distribution were 7.07% (Tl), 0.01% (As), 12.2% (Pb) and 30.2% (O), respectively. The results indicated that Tl was highly accumulated on micro/nano-scale particle of the mine tailings. According to the analysis of d-spacing and axis degrees, the major mineralogical component of tailings particle were avicennite (Tl_2O_3) and thalcusite ($Cu_3Tl_2FeS_4$).

Further analysis of LA-ICP-MS mapping (third row in Fig. 3) confirmed that the mine tailings particle (100 μm) contained high concentrations of As, Tl, Pb and Zn. The contents of As, Tl, Pb and Zn were in

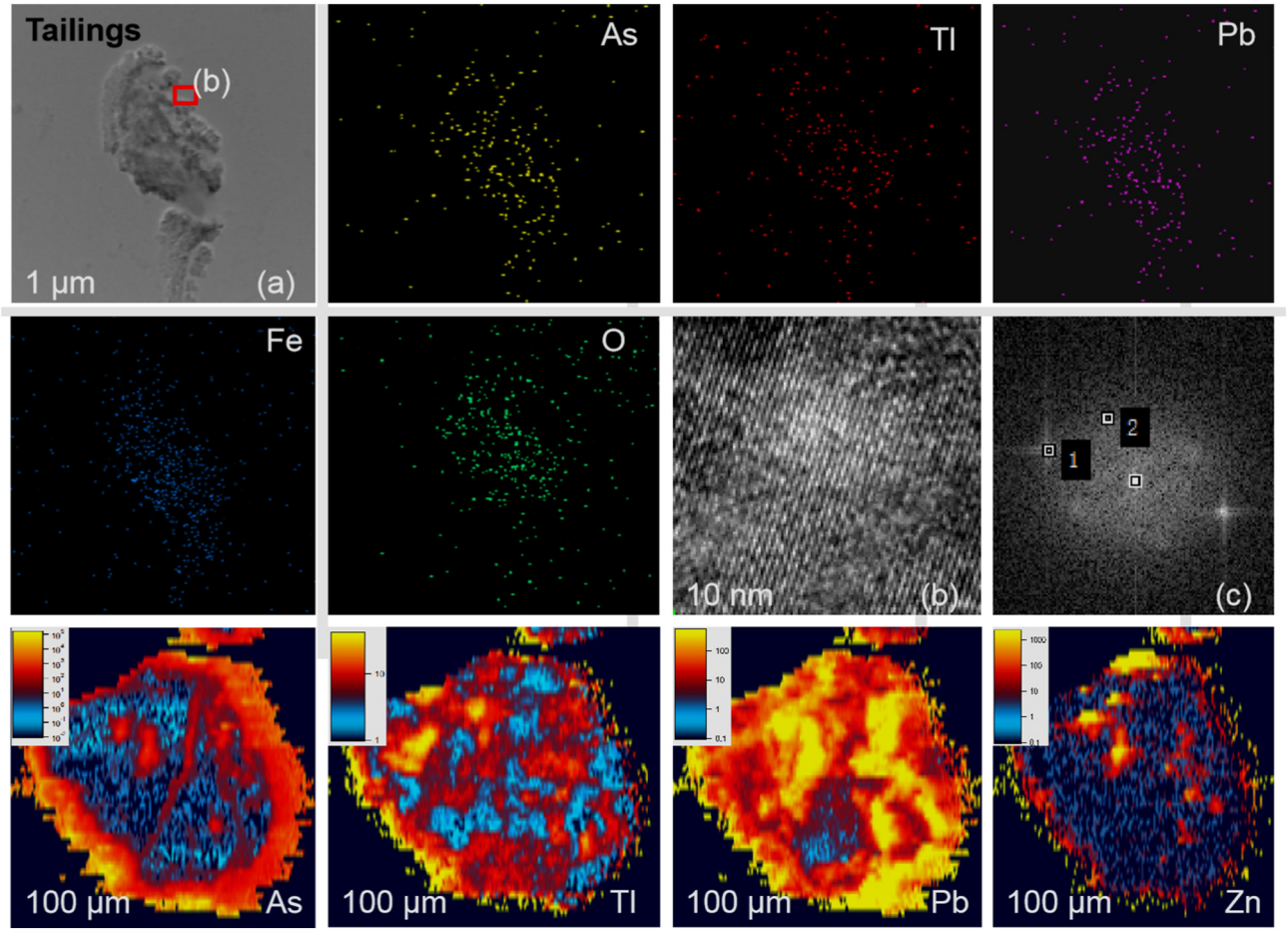

Fig. 3. TEM and LA-ICP-MS mapping of mine tailing: (a) TEM image; (b) HRTEM image; (c) FFT image EM maps of particle.

range of 10–100,000 mg/kg, 1–100 mg/kg, 10–1000 mg/kg and 10–1000 mg/kg, respectively. Pb was distributed most evenly on the particle, while As was mainly concentrated at the edge and Tl was more concentrated in the center. The results further indicated that trace elements Tl and As were highly concentrated in the mine tailings, which might be transformed and transported down the vertical soil profile and into the surrounding environment.

3.4. TEM analysis of soils

As displayed in Fig. 4, Tl, As and Pb on particles (1 μm) of the topsoil (0–20 cm) and mid soil layer (80–100 cm) were well-distributed, with 0.01% (Tl), 0.33% (As) and 0.01% (Pb) of topsoil and 0.01% (Tl), 0.40% (As) and 0.01% (Pb) of mid soil layer, respectively. Apart from the above-mentioned trace elements, the results also showed that Fe and O were highly accumulated, with 6.16% (Fe) and 90.8% (O) of topsoil and 13.4% (Fe) and 82.1% (O) of mid soil. The results of Fe and O accumulating on the particles of Tl-rich soils were consistent with previous findings that Tl enrichment in soils was closely related to iron oxide minerals (Liu et al., 2020a; Wick et al., 2020).

Analytical results of HRTEM images (Fig. 4) revealed that main mineralogical compositions of the topsoil and mid soil layer were thalcusite ($Cu_3Tl_2FeS_4$) and hematite (Fe_2O_3). The mineral - thalcusite ($Cu_3Tl_2FeS_4$) may be inherited from the residual sulfide mineral of the tailing, which is embedded in the inner-sphere of the soil particles. It was reported that thalcusite was subdivided into the solid phase systems Tl-S-O (containing native Tl, carlinite (Tl_2S) and avicennite (Tl_2O_3)) and Fe-S-O (containing native Fe, pyrrhotite, pyrite, magnetite and hematite) (Pekov and Agakhanov, 2008; Karup-Møller and Makovicky, 2011; Hettmann et al., 2014). Hematite (Fe_2O_3) found in the mid soil layer coincided with the previous finding that Tl enrichment in soil was closely related to iron oxide (e.g. Tl adsorption onto hematite particles. In addition, Tl(I) can be oxidized by light-dependent iron cycle and incorporation of Tl(III) and hematite facilitates Tl stabilization into the reducible fraction (Voegelin et al., 2015; Lin et al., 2020; Liu et al., 2020a). The results indicated that enriched levels of Tl and As in the contaminated soil profile were mainly generated from the Tl-As rich mine tailings. The presence of hematite (Fe_2O_3) found in the soil may reflect the enrichment of Tl in the reducible fraction via bonding with Fe-O minerals (Twining et al., 2003; Aguilar-Carrillo et al., 2018).

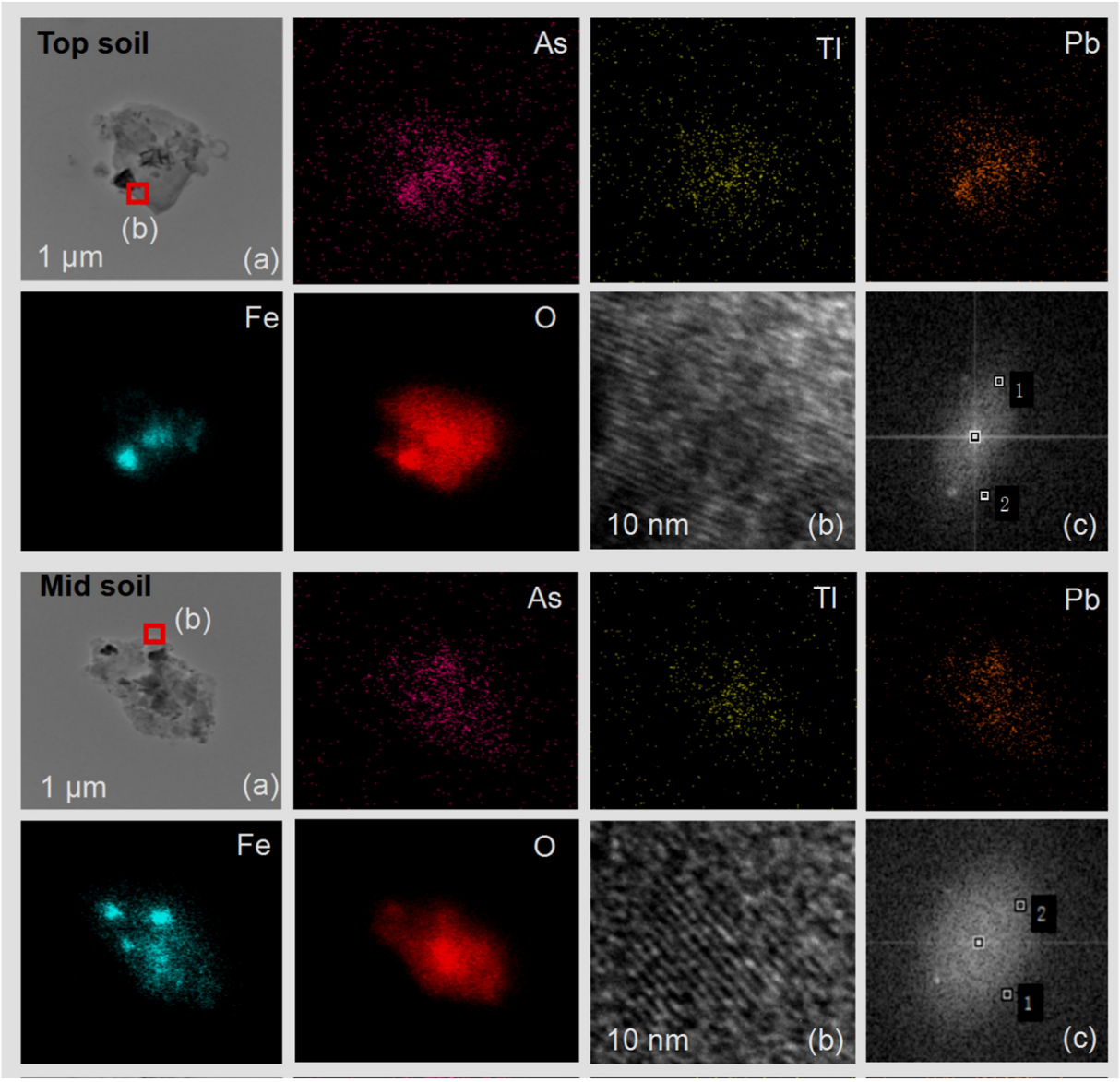

Fig. 4. TEM maps of particles in top soil (0–20 cm) and mid soil (80–100 cm): (a) TEM image; (b) HRTEM image; (c) FFT image EM maps of particle.

3.5. XPS analysis of Tl, As and Fe

XPS analysis was conducted to figure out the speciations of Tl, As and Fe. Thallium in the natural environment usually exists in two oxidation states, monovalent (Tl(I)) and trivalent (Tl(III)) (George et al., 2018; Wang et al., 2018b). The results revealed that Tl was primarily distributed as Tl(I) (peak at about 119 eV), with 73.8%, 78.4%, 75.8%, 79.3%, 82.6% and 80.3% in the soils of 0–20 cm, 20–40 cm, 80–100 cm, 100–120 cm, 160–180 cm and 180–200 cm, respectively (Fig. 5 a1, a2, b1, b2, c1 and c2). In addition, the proportions of Tl(III) (peak at about 118 eV) in the top/mid/bottom soil layers were 21.6%–26.2%, 20.7%–24.2% and 17.4%–19.7%, suggesting a slight decrease from top to bottom. Based on the thermochemical data, Tl(I) is the dominant oxidation state in the natural environment (D'Orazio et al., 2017). However, Tl(I) can be also oxidized to Tl(III) by extreme oxidizing conditions such as sunlight irradiation (UV), interaction with Mn(IV) oxides and light-dependent iron cycle (Twining et al., 2003; Karlsson et al., 2006; Biagioni et al., 2017). Besides, Tl oxidation can also be supported by the action of Tl-oxidizing bacteria, might be the Tl-oxidizing microbiological processes around the rhizospheric area of some wild plants (*e.g.* brake ferns) here in the studied soil (Wei et al., 2020).

As in the soils appeared in both As(III) and As(V) (Fig. 5). The results revealed As(V) (peak at about 45.5 eV) in the soils of 0–20 cm, 20–40 cm, 80–100 cm, 100–120 cm, 160–180 cm and 180–200 cm (Fig. 5 a3, a4, b3, b4, c3 and c4) were 57.1%, 52.0%, 46.0%, 43.5%, 49.2% and 44.5%, respectively. Previous studies indicated that As released from mine ores and tailings could be oxidized under natural weathering (Hammond et al., 2018). It was obvious that As(V) in the topsoil accounted for more than 50% of total As. As displayed in Fig. S3, Fe in soil existed mainly as Fe(III) (peak at about 711 eV), with about 84% in the topsoil. The results revealed that iron in the soil profile was dominantly trivalent and were consistent with the TEM results (hematite (Fe_2O_3) in the soil). Large amount of As(V) and Fe(III) indicating that the topsoil presents the most oxidizing environment, thus supporting the observed oxidation of Tl(I) to Tl(III).

As shown in Table 1, Mn in the soil was only about 800 mg/kg, much less than Fe (5%). No significant evidence of oxidizing participation of Mn (hydr)oxides in Tl geochemical process indicates that there may be negligible effect from Mn(hydr)oxides herein. However, Tl(III) in the studied vertical soil profile might be induced whether by light-dependent oxidation of Fe minerals, or by the action of Tl-oxidizing bacteria. It was reported that trivalent Tl may be stabilized by colloid formation or sorption to Fe oxides (Antić-Mladenović et al., 2017). The XPS results of the soils confirmed a higher percentage of Tl (III) in the topsoil, along with the hematite (Fe_2O_3) found by TEM analysis. Therefore, Tl(III) adsorption onto/incorporation with Fe_2O_3 may promote enrichment of Tl in the reducible fraction.

As mentioned in Section 3.2, Tl in the reducible fraction was the main contribution of geochemical mobile fractions, especially in the topsoil. Therefore, a predominant Tl in the reducible fraction in the

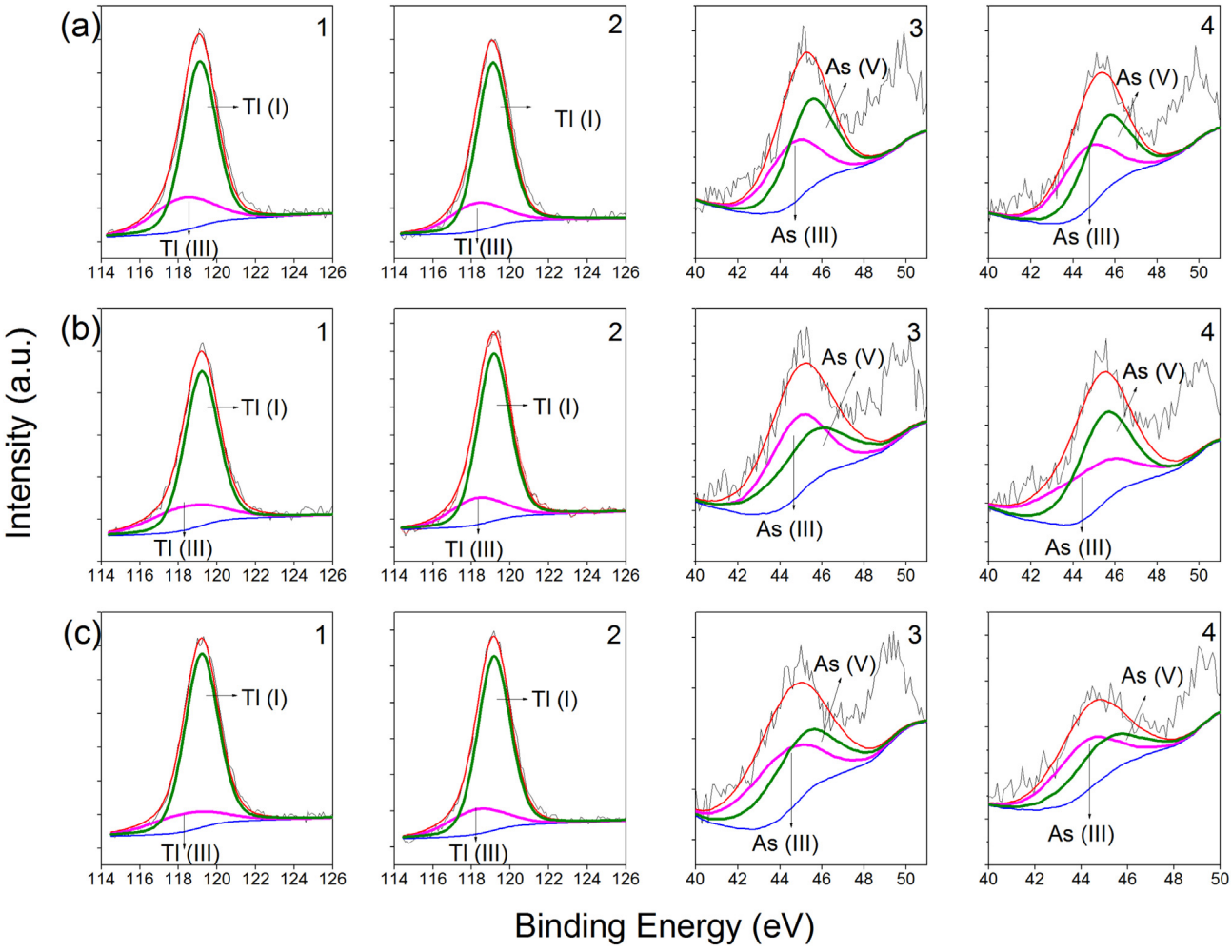

Fig. 5. XPS spectra of As 3d and Tl 4f of the top soil (a1 and a3, 0–20 cm; a2 and a4 20–40 cm), mid soil (b1 and b3, 80–100 cm; b2 and b4 100–120 cm) and bottom soil (c1 and c3, 160–180 cm; c2 and c4 180–200cm).

topsoil, activated by oxidization of Fe oxides may enhance rapid migration and enrichment of Tl in soil and provoke regional Tl pollution. Moreover, once the groundwater level rises or the soil redox potential changes, more Tl will be activated into geochemically mobile fractions and thus pose great potential threat to the groundwater source in the long run. The findings demonstrate that surface oxidation by Fe oxides in mining affected soils may play a pivotal role in Tl mobility and migration, which is vital to control Tl pollution in soil.

4. Conclusions

In this study, remarkably toxic trace elements of Tl (3.91–17.3 mg/kg), As (1830–8840 mg/kg) and Pb (364–1620 mg/kg) were found highly co-enriched in the mine tailings affected soils in Yunnan, Southwestern China. The LA-ICP-MS and TEM results revealed the distribution of Tl and As on specific mineral particles (e.g. Tl_2O_3, $Cu_3Tl_2FeS_4$ and Fe_2O_3) and suggested that Tl in the soils was generated from mining and the stacking of mine tailings. It should be noted that about 50% of Tl in geochemically mobile fractionation was observed in the topsoil, which was mostly enriched in the reducible fraction (29%), representing high migration capability and potential environmental risks. The findings demonstrate that mining activities, participation of Fe-O minerals combined with Tl oxidation in soils may activate and release geochemically mobile Tl fractions into the environmental matrix and cause potentially ecological hazards.

CRediT authorship contribution statement

Xudong Wei: Writing – original draft, Methodology, Formal analysis, Investigation, Visualization. **Jin Wang:** Writing – review & editing. **Jingye She:** Writing – review & editing. **Jing Sun:** Writing – review & editing. **Juan Liu:** Supervision, Writing – review & editing, Funding acquisition. **Yuxuan Wang:** Writing – review & editing. **Xiao Yang:** Writing – review & editing. **Qi"en Ouyang:** Writing – review & editing. **Yuyang Lin:** Writing – review & editing. **Tangfu Xiao:** Writing – review & editing. **Daniel C.W. Tsang:** Writing – review & editing.

Declaration of competing interest

The authors declare that they have no known competing financial interests or personal relationships that could have appeared to influence the work reported in this paper.

Acknowledgments

The work was supported by the National Natural Science Foundation of China (No. 41873015, 41830753 and 41773011), the Guangdong Provincial Natural Science Foundation (2021B1515020078, 2021A1515011588 and 2014A030313527), Scientific Research Projects in Colleges and Universities of Guangzhou Education Bureau, Guangzhou, China (201831803), and the “Challenge Cup” Undergraduate Program (team leader: Yuxuan Wang).

Appendix A. Supplementary data

Supplementary data to this article can be found online at https://doi.org/10.1016/j.scitotenv.2021.146995.

References

Aguilar-Carrillo, J., Herrera, L., Gutiérrez, E.J., Reyes-Domínguez, I.A., 2018. Solid-phase distribution and mobility of thallium in mining-metallurgical residues: environmental hazard implications. Environ. Pollut. 243, 1833–1845.

Alloway, 2015. Heavy metals in soils. Mineral. Mag. 55, 1318–1324.

Alvarenga, I.F.S., Santos, F.E.D., Silveira, G.L., Andrade-Vieira, L.F., Guilherme, L.R.G., 2019. Investigating arsenic toxicity in tropical soils: a cell cycle and DNA fragmentation approach. Sci. Total Environ. 698, 134272.

Antić-Mladenović, S., Frohne, T., Kresović, M., Stärk, H.J., Savić, D., Ličina, V., Rinklebe, J., 2017. Redox-controlled release dynamics of thallium in periodically flooded arable soil. Chemosphere 178, 268–276.

Beiyuan, J., Awad, Y.M., Beckers, F., Tsang, D.C.W., Ok, Y.S., Rinklebe, J., 2017a. Mobility and phytoavailability of As and Pb in a contaminated soil using pine sawdust biochar under systematic change of redox conditions. Chemosphere 178, 110–118.

Beiyuan, J., Li, J., Tsang, D.C.W., Wang, L., Poon, C.S., Li, X.D., Fendorf, S., 2017b. Fate of arsenic before and after chemical-enhanced washing of an arsenic-containing soil in Hong Kong. Sci. Total Environ. 599-600, 679–688.

Belzile, N., Chen, Y.W., 2017. Thallium in the environment: a critical review focused on natural waters, soils, sediments and airborne particles. Appl. Geochem. 84, 218–243.

Besold, J., Biswas, A., Suess, E., Scheinost, A.C., Rossberg, A., Mikutta, C., Kretzschmar, R., Gustafsson, J.P., Planer-Friedrich, B., 2018. Monothioarsenate transformation kinetics determining arsenic sequestration by sulfhydryl groups of peat. Environ. Sci. Technol. 52, 7317–7326.

Biagioni, C., D'Orazio, M., Lepore, G.O., D'Acapito, F., Vezzoni, S., 2017. Thallium-rich rust scales in drinkable water distribution systems: a case study from northern Tuscany, Italy. Sci.Total Environ. 587, 491–501.

Briki, M., Zhu, Y., Gao, Y., Shao, M., Ji, H., 2017. Distribution and health risk assessment to heavy metals near smelting and mining areas of Hezhang, China. Environ. Monit. Assess. 189, 458.

Carrizales, L., Razo, I., Téllez-Hernández, J.I., Torres-Nerio, R., Torres, A., Batres, L.E., Cubillas, A., Díaz-Barriga, F., 2006. Exposure to arsenic and lead of children living near a copper-smelter in San Luis Potosi, Mexico: importance of soil contamination for exposure of children. Environ. Res. 101, 1–10.

CEMS (The Chinese Environmental Monitoring Station), 1990. The background values of elements in the Chinese soil. China Environ. Sci. (in Chinese).

Cortada, U., Hidalgo, M.C., Martínez, J., Rey, J., 2018. Impact in soils caused by metal(loid)s in lead metallurgy. The case of La Cruz Smelter (Southern Spain). J. Geochem. Explor. 190, 302–313.

D'Orazio, M., Biagioni, C., Dini, A., Vezzoni, S., 2017. Thallium-rich pyrite ores from the Apuan Alps, Tuscany, Italy: constraints for their origin and environmental concerns. Mineral. Deposita 52, 687–707.

Downs, R.T., Hall-Wallace, M., 2003. The American mineralogist crystal structure database. Am. Mineral. 88, 247–250.

George, L.L., Cook, N.J., Crowe, B.B.P., Ciobanu, C.L., 2018. Trace elements in hydrothermal chalcopyrite. Miner. Mag. 82, 59–88.

George, L.L., Biagioni, C., Lepore, G.O., Lacalamita, M., Agrosì, G., Capitani, G.C., Bonaccorsi, E., d'Acapito, F., 2019. The speciation of thallium in (Tl,Sb,As)-rich pyrite. Ore Geol. Rev. 107, 364–380.

Ghezzi, L., D'Orazio, M., Doveri, M., Lelli, M., Petrini, R., Giannecchini, R., 2019. Groundwater and potentially toxic elements in a dismissed mining area: thallium contamination of drinking spring water in the Apuan Alps (Tuscany, Italy). J. Geochem. Explor. 197, 84–92.

Guo, J., Cao, Y., Luo, Z., Fang, H., Chen, Z., Wang, D., Xu, F., Yan, C., 2018. Distribution, fractions, and potential release of thallium in acidic soils nearby a waste copper mining site from southern China. Environ. Sci. Pollut. Res. 25, 17980–17988.

Hammond, C.M., Root, R.A., Maier, R.M., Chorover, J., 2018. Mechanisms of arsenic sequestration by Prosopis juliflora during the phytostabilization of metalliferous mine tailings. Environ. Sci. Technol. 52, 1156–1164.

Hettmann, K., Marks, M.A.W., Kreissig, K., Zackc, T., Wenzel, T., Rehkämper, M., Jacob, D.E., Markl, G., 2014. The geochemistry of Tl and its isotopes during magmatic and hydrothermal processes: the peralkaline ilimaussaq complex, southwest greenland. Chem. Geol. 366, 1–13.

Huang, X., Li, N., Wu, Q., Long, J., Luo, D., Huang, X., Li, D., Zhao, D., 2018. Fractional distribution of thallium in paddy soil and its bioavailability to rice, Ecotox. Environ. Safe. 148, 311–317.

Karlsson, U., Karlsson, S., Düker, A., 2006. The effect of light and iron(II)/iron(III) on the distribution of Tl(I)/Tl(III) in fresh water systems. J. Environ. Monit. 8, 634–640.

Karup-Møller, S., Makovicky, E., 2011. Mineral X, a new thalcusite homologue from the IlÃmaussaq complex, South Greenland. Bull. Geol. Soc. Den. 59, 13–22.

Kaya, C., Ashraf, M., Alyemeni, M.N., Corpas, F.J., Ahmad, P., 2020. Salicylic acid-induced nitric oxide enhances arsenic toxicity tolerance in maize plants by upregulating the ascorbate-glutathione cycle and glyoxalase system. J. Hazard. Mater. 399, 123020.

Lee, J.H., Kim, D.J., Ahn, B.K., 2015. Distributions and concentrations of thallium in Korean soils determined by single and sequential extraction procedures. B. Environ. Contam. Tox. 94, 756–763.

Li, N., Zhou, Y., Liu, J., Tsang, D.C.W., Wang, J., She, J., Zhou, Y., Yin, M., Chen, Z., Chen, D., 2020. Persistent thallium contamination in river sediments, source apportionment and environmental implications. Ecotox. Environ. Safe. 202, 110874.

Lin, J., Yin, M., Wang, J., Liu, J., Tsang, D.C.W., Wang, Y., Lin, M., Li, H., Zhou, Y., Song, G., Chen, Y., 2020. Geochemical fractionation of thallium in contaminated soils near a large-scale Hg-Tl mineralised area. Chemosphere 239, 124775.

Liu, J., Luo, X., Wang, J., Xiao, T., Chen, D., Sheng, G., Yin, M., Lippold, H., Wang, C., Chen, Y., 2017. Thallium contamination in arable soils and vegetables around a steel plant-a newly-found significant source of Tl pollution in South China. Environ. Pollut. 224, 445–453.

Liu, J., Wang, J., Tsang, D.C.W., Xiao, T., Chen, Y., Hou, L., 2018. Emerging thallium pollution in China and source tracing by thallium isotopes. Environ. Sci. Technol. 52, 11977–11979.

Liu, J., Luo, X., Sun, Y., Tsang, D.C.W., Qi, J., Zhang, W., Li, N., Yin, M., Wang, J., Lippold, H., Chen, Y., Sheng, G., 2019a. Thallium pollution in China and removal technologies for waters: a review. Environ. Int. 126, 771–790.

Liu, J., Yin, M., Luo, X., Xiao, T., Wu, Z., Li, N., Wang, J., Zhang, W., Lippold, H., Belshaw, N., Feng, Y., Chen, Y., 2019b. The mobility of thallium in sediments and source apportionment by lead isotopes. Chemosphere 219, 864–874.

Liu, J., Wei, X., Zhou, Y., Tsang, D.C.W., Bao, Z., Lippold, H., Yuan, W., Wang, J., Feng, Y., Chen, D., 2020a. Thallium contamination, health risk assessment and source apportionment in common vegetables. Sci. Total Environ. 703, 135547.
Liu, J., Zhou, Y., She, J., Tsang, D.C.W., Lippold, H., Wang, J., Jiang, Y., Wei, X., Yuan, W., Luo, X., Zhai, S., Song, L., 2020b. Quantitative isotopic fingerprinting of thallium associated with potentially toxic elements (PTEs) in fluvial sediment cores with multiple anthropogenic sources. Environ. Pollut. 266, 115252.
Liu, J., Ren, J., Zhou, Y., Tsang, D.C., Lin, J., Yuan, W., Wang, J., Yin, M., Wu, Y., Xiao, T., Chen, Y., 2020c. Effects and mechanisms of mineral amendment on thallium mobility in highly contaminated soils. J. Environ. Manage. 262, 110251.
Liu, J., Yin, M., Xiao, T., Zhang, C., Tsang, D., Bao, Z., Zhou, Y., Chen, Y., Luo, X., Yuan, W., Wang, J., 2020d. Thallium isotopic fractionation in industrial process of pyrite smelting and environmental implications. J. Hazard. Mater. 384, 121378.
Liu, J., Ren, S., Cao, J., Tsang, D, Beiyuan, J., Peng, Y., Fang, F., She, J., Yin, M., Shen, N., Wang, J., 2021. Highly efficient removal of thallium in wastewater by $MnFe_2O_4$-biochar composite. J. Hazard. Mater. 401, 123311.
López-Arce, P., Garrido, F., García-Guinea, J., Voegelin, A., Göttlicher, J., Nieto, J., 2019. Historical roasting of thallium- and arsenic-bearing pyrite: current Tl pollution in the Riotinto mine area. Sci. Total Environ. 648, 1263–1274.
Lukaszewski, Z., Jakubowska, M., Zembrzuski, W., 2018. The mobility of thallium from bottom soil of the Silesian-Cracowian zinc-lead ore deposit region (Poland). J. Geochem. Explor. 184, 11–16.
Meharg, A.A., Rahman, M.M., 2003. Arsenic contamination of Bangladesh paddy field soils: implications for rice contribution to arsenic consumption. Environ. Sci. Technol. 37, 229–234.
Pekov, I.V., Agakhanov, A.A., 2008. Thallium-rich murunskite from the lovozero pluton, kola peninsula, and partitioning of alkali metals and thallium between sulfide minerals. Geol. Ore Deposit. 50, 583–589.
Qi, J., Lai, Y., Liang, C., Yan, S., Huang, K., Pan, W., Feng, L., Jiang, L., Zhu, P., Hao, J., Tong, S., Tao, F., 2019. Prenatal thallium exposure and poor growth in early childhood: a prospective birth cohort study. Environ. Int. 123, 224–230.
Rahman, M.A., Rahman, A., Khan, M., Kaiser, Zaved, Renzaho, Andre M.N., 2018. Human health risks and socio-economic perspectives of arsenic exposure in Bangladesh: a scoping review. Ecotox. Environ. Safe. 150, 335–343.
Rocke, R.B.A., 2013. John parascandola.king of poisons: a history of arsenic. Isis 104, 829.
SEP and GAQIQ (State Environmental Protection Administration of the P.R. China & General Administration of Quality Supervision, Inspection and Quarantine of the P. R. China), 2015. Chinese National Standards (GB 15618-2015). Soil Environ. Qual. Stand. Agric. Land 7–12 (in Chinese).
Sun, J., Bostick, B., Mailloux, B., Ross, J., Chillrud, S., 2016. Effect of oxalic acid treatment on sediment arsenic concentrations and lability under reducing conditions. J. Hazard. Mat. 311, 125–133.
Sun, J., Mailloux, B., Chillrud, S., van Geen, A., Thompson, A., Bostick, B., 2018. Simultaneously quantifying ferrihydrite and goethite in natural sediments using the method of standard additions with X-ray absorption spectroscopy. Chem. Geol. 476, 248–259.
Twining, B.S., Twiss, M.R., Fisher, N.S., 2003. Oxidation of thallium by freshwater plankton communities. Environ. Sci. Technol. 37, 2720–2726.
Vaněk, A., Chrastný, V., Komárek, M., Penížek, V., Teper, L., Cabala, J., Drábek, O., 2013. Geochemical position of thallium in soils from a smelter-impacted area. J. Geochem. Explor. 124, 176–182.
Vaněk, A., Grösslová, Z., Mihaljevič, M., Trubač, J., Ettler, V., Teper, L., Cabala, J., Rohovec, J., Zádorová, T., Penížek, V., Pavlů, L., Holubík, O., Němeček, K., Houška, J., Drábek, O., Ash, C., 2016. Isotopic tracing of thallium contamination in soils affected by emissions from coal-fired power plants. Environ. Sci. Technol. 50, 9864–9871.
Vaněk, A., Grösslová, Z., Mihaljevič, M., Ettler, V., Trubač, J., Chrastný, V., Penížek, V., Teper, L., Cabala, J., Voegelin, A., Zádorová, T., Oborná, V., Drábek, O., Holubík, O., Houška, J., Pavlů, L., Ash, C., 2018. Thallium isotopes in metallurgical wastes/contaminated soils: a novel tool to trace metal source and behavior. J. Hazard. Mater. 343, 78–85.
Vaněk, A., Holubik, O., Oborná, V., Mihaljevič, M., Trubač, J., Ettler, V., Pavlů, L., Vokurková, P., Penížek, V., Zádorová, T., Voegelin, A., 2019. Thallium stable isotope fractionation in white mustard: implications for metal transfers and incorporation in plants. J. Hazard. Mater. 369, 521–527.
Verma, G., Srivastava, D., Narayan, S., Shirke, P.A., Chakrabarty, D., 2020. Exogenous application of methyl jasmonate alleviates arsenic toxicity by modulating its uptake and translocation in rice (Oryza sativa L.). Ecotox. Environ. Safe. 201, 110735.
Voegelin, A., Pfenninger, N., Petrikis, J., Majzlan, J., Ploetze, M., Senn, A.C., Mangold, S., Steininger, R., Göttlicher, J., 2015. Thallium speciation and extractability in a thallium- and arsenic-rich soil developed from mineralized carbonate rock. Environ. Sci. Technol. 49, 5390.
Wang, Y., We, F., Yang, G., Zheng, C., Wu, Y., Zheng, S., Elemental chemistry of soil environment, China Environ. Sci. 1995 (in Chinese).
Wang, J., Xing, Y., Li, P., Xia, J., Liu, T., Feng, X., 2018a. Chemically-assisted phytoextraction from metal(loid)s-polluted soils at a typical carlin-type gold mining area in southwest China. J. Clean. Prod. 189, 612–619.
Wang, Z., Zhang, B., Jiang, Y., Li, Y., He, C., 2018b. Spontaneous thallium (I) oxidation with electricity generation in single-chamber microbial fuel cells. Appl. Energ. 209, 33–42.
Wang, L., Chen, L., Guo, B., Tsang, D.C.W., Huang, L., Ok, Y.S., Mechtcherine, V., 2020a. Red mud-enhanced magnesium phosphate cement for remediation of Pb and As contaminated soil. J. Hazard. Mater. 400, 123317.
Wang, J., Zhou, Y., Dong, X., Yin, M., Tsang, D., Sun, J., Liu, J., Song, G., Liu, Y., 2020b. Temporal sedimentary record of thallium pollution in an urban lake: an emerging thallium pollution source from copper metallurgy. Chemosphere 242, 125172.
Wang, J., She, J., Zhou, Y., Tsang, D., Beiyuan, J., Xiao, T., Dong, X., Chen, Y., Liu, J., Yin, M., Wang, L., 2020c. Microbial insights into the biogeochemical features of thallium occurrence: A case study from polluted river sediments. Sci. Total Environ. 739, 139957.
Wang, J., Wang, L., Wang, Y., Tsang, D., Yang, X., Beiyuan, J., Yin, M., Xiao, T., Jiang, Y., Lin, W., Zhou, Y., Liu, J., Wang, L., Zhao, M., 2021a. Emerging risks of toxic metal(loid)s in soil-vegetables influenced by steel-making activities and isotopic source apportionment. Environ. Int. 146, 106207.
Wang, J., Yin, M., Liu, J., Shen, C.-C., Yu, T.-L., Li, H.-C., Zhong, Q., Sheng, G., Lin, K., Jiang, X., Dong, H., Liu, S., Xiao, T., 2021b. Geochemical and U-Th isotopic insights on uranium enrichment in reservoir sediments. J. Hazard. Mater. 414, 125466.
Wei, X., Zhou, Y., Tsang, D.C.W., Zhang, C., Yin, M., Liu, J., Xiao, T., Feng, Y., 2020. Hyperaccumulation and transport mechanism of thallium and arsenic in brake ferns (Pteris vittata L.): a case study from mining area. J. Hazard. Mater. 388, 121756.
Wick, S., Baeyens, B., Fernandes, M.M., Gttlicher, J., Fischer, M., Pfenninger, N., Plötze, M., Voegelin, A., 2020. Thallium sorption and speciation in soils: role of micaceous clay minerals and manganese oxides. Geochim. Cosmochim. Ac. 288, 83–100.
Wu, S., Yang, D., Zhou, Y., Zhou, H., Ai, S., Yang, Y., Wan, Z., Luo, L., Tang, L., Tsang, D.C.W., 2020. Simultaneous degradation of *p*-arsanilic acid and inorganic arsenic removal using M-rGO/PS Fenton-like system under neutral conditions. J. Hazard. Mater. 399, 123032.
Xiao, T., Boyle, D., Guha, J., Rouleau, A., Hong, Y., Zheng, B., 2003. Groundwater-related thallium transfer processes and their impacts on the ecosystem: southwest Guizhou Province, China. Appl. Geochem. 18, 675–691.
Xiao, T., Yang, F., Li, S., Zheng, B., Ning, Z., 2012. Thallium pollution in China: a geo-environmental perspective. Sci. Total Environ. 421–422, 51–58.
Yang, C., Chen, Y., Peng, P., Li, C., Chang, X., Xie, C., 2005. Distribution of natural and anthropogenic thallium in the soils in an industrial pyrite slag disposing area. Sci. Total Environ. 341, 159–172.
Yin, M., Sun, J., Chen, Y., Wang, J., Shang, J., Belshaw, N., Shen, C., Liu, J., Li, H., Linghu, W., Xiao, T., Dong, X., Song, G., Xiao, E., Chen, D., 2019. Mechanism of uranium release from uranium mill tailings under long-term exposure to simulated acid rain: geochemical evidence and environmental implication. Environ. Pollut. 244, 174–181.
Yin, M., Tsang, D., Sun, J., Wang, J., Shang, J., Fang, F., Liu, J., Song, G., Xiao, T., Chen, D., 2020. Critical insight and indication on particle size effects towards uranium release from uranium mill tailings: Geochemical and mineralogical aspects. Chemosphere 250, 126315.
Yin, M., Zhou, Y., Tsang, D., Beiyuan, J., Song, L., She, J., Wang, J., Zhu, L., Fang, F., Wang, L., Liu, J., Liu, Y., Song, G., Chen, D., Xiao, T., 2021. Emergent thallium exposure from uranium mill tailings. J. Hazard. Mater. 407, 124402.
Zhou, T., Fan, Y., Yuan, F., Cooke, D., Zhang, X., Li, L., 2007. A preliminary investigation and evaluation of the thallium environmental impacts of the unmined Xiangquan thallium-only deposit in Hexian, China. Environ. Geol. 54, 131–145.
Zhou, Y., Wang, J., Wei, X., Ren, S., Yang, X., Beiyuan, J., Wei, L., Liu, J., She, J., Zhang, W., Liu, Y., Xiao, T., 2021. Escalating health risk of thallium and arsenic from farmland contamination fueled by cement-making activities: A hidden but significant source. Sci. Total Environ. 782, 146603.